Hybrid Aperture Modulation for THz Imaging with Compressive Sensing

Joachim H.G. Ender
Center for Sensor Systems ZESS, University of Siegen
and Fraunhofer Institute for High Frequency Physics and Radar Techniques FHR, Wachtberg, Germany
Peter Knott
Institute for High Frequency Techniques, Technical University of Aachen (RWTH)
and Fraunhofer Institute for High Frequency Physics and Radar Techniques FHR, Wachtberg, Germany

***Abstract*—In this paper, we describe a method for THz imaging following the principle of the *single-pixel camera* [1] where the aperture modulation is done with two concentrically rotating code-disks, i.e. the analogue rotation is combined with the digital spatial code applied to the disks - that is the reason why we call this principle *hybrid aperture modulation*. Besides signal modelling and simulation results we will also describe an experimental THz radar system which is built up for the proof of concept. Because of its similarity to a roulette machine (in two aspects: rotating disk + random variables) we will also call it *roulette radar*. The motivation for this approach was to investigate an extremely simple THz imaging device with no mechanical moving parts except small light-weight disks rotating with constant angular velocities - like the disk in a PC!**

I. Introduction

In 2008 the principle of *single pixel camera* was first introduced [1] for optical applications. The center idea is to apply a sequence of digitally steered random masks in the optical focusing chain to gather the wave from the modulated aperture in a single detector (see Fig. 1) and to recover the image from the sequence of measurements with compressive sensing algorithms. Mathematically, this is an implementation of the *principle of random projections* which was elaborated within the theory of compressive sensing [2]. Later the technique of the single pixel camera was transferred to THz imaging [3], [4]. Instead of the micro-mirror masking device here a semiconductor-based optical switch is used to generate the sequence of masks.

In this paper, we describe a method for THz imaging following the principle of single-pixel camera, too, but the aperture modulation is done with two concentrically rotating code-disks. A rotating disk (*spinning disk*) was also introduced in [5] for infrared imaging, but there are major differences to our approach; especially a novelty is the implementation of two (or more) disks which is necessary to achieve a larger number of pixels for the resulting images.

II. Modelling of the General Random Projection Approach

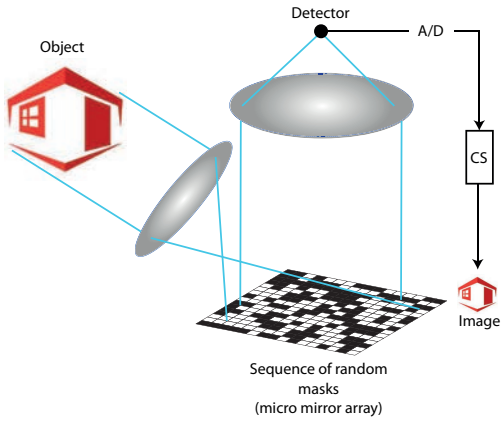

Fig. 1. *The principle of single-pixel imaging*

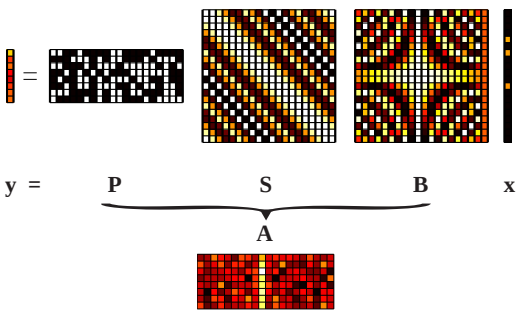

Fig. 2. *Signal flow from features to measurements*

For the modelling of a random projection the following model is used, as illustrated in Fig. 2:

$$\mathbf{y} = \mathbf{PSBx} + \mathbf{n} \tag{1}$$

where $\mathbf{x}$ is a sparse vector describing the coefficients in a feature base matrix $\mathbf{B}$ (e.g. a wavelet base). The product $\boldsymbol{\rho} = \mathbf{Bx}$ characterizes the amplitude distribution on the surface of the object we want to image. The physical signal model how a point-like amplitude transfers to a sensor

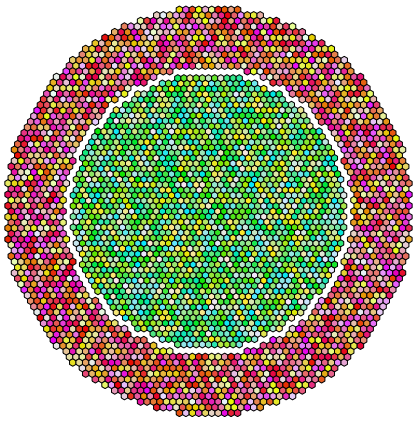

Fig. 3. *Initial design of the distribution of the elementary reflectors*

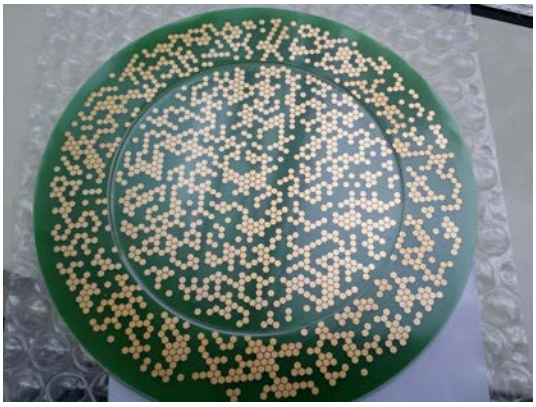

Fig. 4. *Realized disks*

reference plane manifests as a column vector of the matrix $\mathbf{S}$. Finally the application of a sequence of masks or a hybrid aperture modulation, respectively, is described by a matrix $\mathbf{P}$ where the row index m denotes the mth measurement which is additional superposed by measurement noise as the mth coefficient of $\mathbf{n}$. Many results of the compressive sensing theory regard independent Bernoulli or Gaussian random variables as entries for the matrix $\mathbf{P}$. In the original single-pixel camera the Bernoulli (+-1 with same probability) variables were generated by a pseudo-random generator and transferred to the micro-mirror device.

Of course, the discrete formulation of the linear dependence from the feature space to the measurement demands also to discretize features, amplitude distribution, and the sensor reference plane into grids.

The matrix product in Eq. (1) can be combined to a single $M \times N$ *sensing matrix* $\mathbf{A} = \mathbf{PSB}$. The recovery of $\mathbf{x}$ from the measurements $\mathbf{y} = \mathbf{Ax}+\mathbf{n}$ with a larger number of unknowns N as measurements M is performed by any approved pursuit, like *basis pursuit denoising (BPDN)* or *orthogonal matching pursuit (OMP)*.

A large part of the literature for compressive sensing is dedicated to the mathematical analysis, recovery guarantees or the probability of recovery, depending on properties of the matrix $\mathbf{A}$, as coherence, restricted isometry property, and so on.

III. Description of the Proposed Coded Disk Device

The heart of our proposed imaging device consists of two concentrically rotating disks each equipped with a hexagonal grid. At the grid points, either an elementary reflector is placed or not present, each with probability $\frac{1}{2}$. The elementary reflectors are copper hexagons etched on the basis material fiberglass (FR-4 material). The radii of the two bounding circles are chosen to get the same expected number of elements in the inner disk and the outer ring. Fig. 3 depicts the first design of the reflect-arrays and Fig. 4 shows a photo of the realized printed disks.

The inner and the outer disks are mechanically coupled by a gearing mechanism in that way that the outer ring performs Q rotations while the inner disk rotes P times. In our design we choose $Q = 6, P = 7$ which are prime to each other. In this case no repetition of the relative angular states of the two disks happens during one period, defined by Q rotations of the outer ring corresponding to P rotations of the inner disk. We remark that the design with more than one disk was necessary to guarantee a sufficient number M of measurements which are independent enough to get a sufficient incoherence of the sensing matrix described in the next section.

The mechanical driving system is shown in Fig. 5. It includes an angular coding unit generating pulses for the synchronization of the radar device.

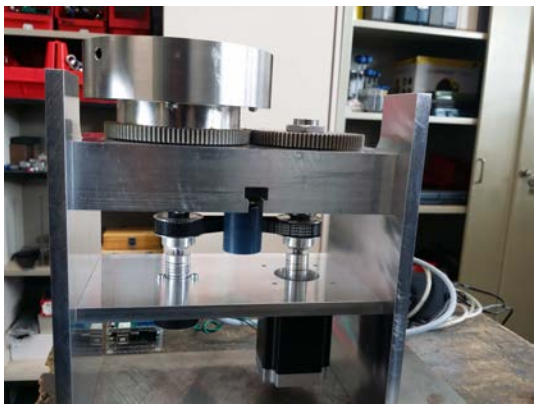

Fig. 5. *A view at the mechanical driving system*

Unfortunately measurements could not be performed before the submission deadline for the final paper.

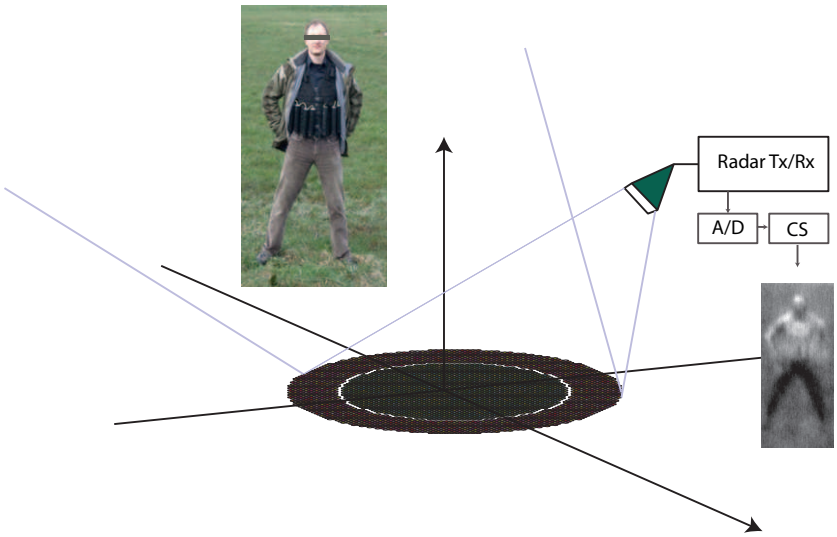

Fig. 6. *Illustration of the radar operation with the rotating disks*

IV. Principle operation of the roulette radar

The code disks are illuminated by a (in our case: millimetric wave) radar under a certain incidence angle. In the basic mode, a monofrequent CW-radar is used. At each single element the wave is reflected with the single reflection diagram maximum at the mirror angle. If each of the grid points would be occupied by a reflector, the reflected waves would add to a pattern with a focused main beam into the direction of the mirror angle with a beamwidth approximal to λ/d where λ is the wavelength and d the diameter of the outer ring. But because of the random thinning of the array the resulting reflection characteristic can be written as a sum of two contributions: first the mentioned focused beam which is independent on the angular state of the disks and a second which would arise from a +/- 1 amplitude modulation which is strongly dependent on this stage.

For each point of the 'scene', i.e. the reflecting object, the Tx wave is reflected scaled with the complex reflection coefficient at this point. In principle, the superposition of all these elementary reflections could be captured by a separate receiving antenna. In this, case, the general model of Eq. (1) directly applies.

In our design we decided to use only one antenna for transmit and receive, i.e. the wave reflected by the object has to undergo the same way back: reflection at the array, then back to the antenna. After demodulation with the carrier frequency, the signal is A/D-converted (clocked by the pulses generated by the mechanical device) and stored. This version can no longer be modeled by the simple linear operations in Eq. (1), since the random projection occurs two times - because of the two reflections at the rotating disks for the forward way to the object and the backward way.

Because of the monofrequent operation there is no primary range resolution. Nevertheless, the recorded echo signal is dependent on range when the scene is closer than the far field condition for the reflect-array. If a radar with a certain bandwidth is operated, e.g. an FMCW-radar, the data rate has to be multiplied with the number of independent frequency samples and the signal processing is complicated significantly.

V. Signal model for the roulette radar

A. The sensing matrix

We regard a Cartesian coordinate system with its origin at the center of the disks and its z-axis orthogonal to the disk plane. Let $\vec{R}_a$ denote the vector to the phase center of the antenna, $\vec{r}_\nu^{(i)}, \nu = 1, \ldots, N_i$ the positions of the reflecting antenna elements of the inner disk, analogue $\vec{r}_\mu^{(o)}, \mu = 1, \ldots, N_o$ the element positions of the outer ring.

Further, let $\varphi_i(T)$ be the rotation angle of the inner disk at slow time T and $\varphi_o(T)$ the same for the outer ring. The matrix

$$\mathbf{L}(\varphi) = \begin{pmatrix} \cos\varphi & -\sin\varphi & 0 \\ \sin\varphi & \cos\varphi & 0 \\ 0 & 0 & 1 \end{pmatrix} \qquad (2)$$

describes the coordinate transform by rotation by φ around the z-axis.

Let $\vec{R}$ be the position of a point of the object. Then the way that the transmitted wave has to travel from the Tx antenna over the νth element of the inner disk - or f over the μth element of the outer disk, respectively - to the object point is

$$
\begin{aligned}
R_\nu^{(i)}(T;\vec{R}) &= \|\mathbf{L}(\varphi_i(T))\vec{r}_\nu^{(i)} - \vec{R}_a\| \\
&\quad + \|\mathbf{L}(\varphi_i(T))\vec{r}_\nu^{(i)} - \vec{R}\| \\
R_\mu^{(o)}(T;\vec{R}) &= \|\mathbf{L}(\varphi_o(T))\vec{r}_\mu^{(o)} - \vec{R}_a\| \\
&\quad + \|\mathbf{L}(\varphi_o(T))\vec{r}_\mu^{(o)} - \vec{R}\|
\end{aligned}
$$

The complex amplitude of the transmitted wave at time T impinging the object point then is the superposition of all partial contributions:

$$
\begin{aligned}
a(T;\vec{R}) &= \sum_{\nu=1}^{N_i} c_\nu^{(i)}(T;\vec{R}) \exp\{-jkR_\nu^{(i)}(T;\vec{R})\} \\
&\quad + \sum_{\mu=1}^{N_o} c_\mu^{(o)}(T;\vec{R}) \exp\{-jkR_\mu^{(o)}(T;\vec{R})\}
\end{aligned}
$$

$c_\nu^{(i)}(T;\vec{R})$ and $c_\mu^{(o)}(T;\vec{R})$ are amplitude factors caused by the antenna characteristics, the backscattering characteristics of the elementary reflectors and the $1/r$-decrease of the electrical field. Since for the way back the same formula applies, the return for a single scatterer at position $\vec{R}$ with unit reflectivity is

$$
s(T;\vec{R}) = a^2(T;\vec{R}) \tag{3}
$$

and the measurement signal is the superposition

$$
y(T) = \int \rho(\vec{R}) s(T;\vec{R}) d\vec{R} + n(T) \tag{4}
$$

where $\rho(\vec{R})$ denotes the reflectivity at position $\vec{R}$.

After digitizing the scene domain and introducing spatial sampling, Eq. (4) is transformed into the sensing equation

$$
\mathbf{y} = \mathbf{S}\boldsymbol{\rho} + \mathbf{n}. \tag{5}
$$

Note that the random projection is already included, since only the positions of the existing reflectors are used. Of course this is a simple 'mathematical' model of the physics, since electromagnetical effects like coupling and multipath are not considered in this paper. Nevertheless, an electromagnetic simulation of the hexagonal mirrors and the complete disks is in progress.

B. Rough estimation of the number of independent measurements

In the following, we will show why we need more than only one disk, driven with different angular velocities. Starting with just one disk, the signal will change over the angle significantly only when the outer elements have changed their positions at least by the order of a quarter wavelength:

$$
\Delta\varphi \frac{d}{2} \geq \frac{\lambda}{4} \tag{6}
$$

So there will be not more than $M \approx \frac{2\pi}{\Delta\varphi} = \frac{4\pi d}{\lambda}$ (more or less independent) samples of the signal during one rotation. On the other hand, the number of independent directions N is roughly given by the area of the disk $A = \pi\frac{d^2}{4}$ divided by the effective area of a single mirror $A_0 = \frac{\lambda^2}{4\pi}G_0$ where G_0 is the gain of the single element;

$$
N \approx \frac{(\pi d)^2}{\lambda^2 G_0} \tag{7}
$$

Obviously, N increases with d^2, while M is proportional only to d. Since N is roughly equal to the number of pixels of the later image, d should be not too small. To get a sufficient reconstruction, the measurement sparsity $\gamma = \frac{M}{N}$ has to be larger or equal to a γ_0. It follows

$$
\gamma \approx \frac{4\pi d}{\lambda}\frac{\lambda^2}{4\pi}G_0 \tag{8}
$$

In our design, the diameter is $d = 128\lambda$, the gain of a single element is $G_0 \approx 20$ leading to

$$
N \approx 8000, \quad M \approx 1600, \gamma \approx 0.2. \tag{9}
$$

This measurement sparsity seems too small for good reconstruction of scenes which are not very sparse. For this reason, we introduced the second disk to get a factor 6 of non redundant measurements. This is in accordance to the performed simulations for one and for two disks, where only the second case showed good results.

Of course, these are only rule-of-the-thumb considerations. A rigid derivation can be performed for the expected correlation of the signals for two different directions over a whole rotation cycle.

VI. Simulation results

Simulations were performed on the basis of Eq. (5) for S-sparse scenes, i.e. S directions with amplitudes unequal to zero. The diameter of the outer ring was chosen to 50 wavelengths, smaller than that of the experimental radar (128 wavelengths) , leading to 936 element positions in the inner disk and 940 in the outer. A grid of directions was defined in the u, v-plane with 1876 points. The number of samples during one rotation cycle was chosen according to a desired incoherence of the sensing matrix to $M = 924$, i.e. a measurement sparsity $\gamma = 0.4925$ and the coherence resulted to 0.4082, which is an acceptable number. Fig. 7 shows the response to a single point reflector over one rotation cycle, which is identical to a columns of the sensing matrix, and the autocorrelation. Though the latter exhibits some larger side lobes, there are no secondary main lobes, showing that the combination of the inner and the outer disk does work well.

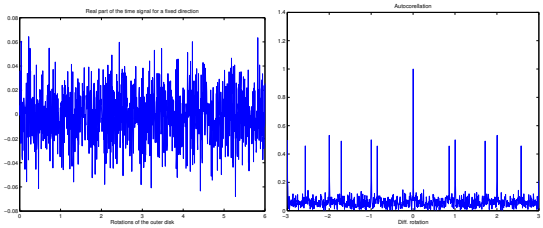

Fig. 7. *Left: Real part of a simulated signal over one rotation cycle for a single point reflector. Right: its autocorrelation function*

Fig. 8 shows a simulated sparse scene where 50 random directions with amplitudes unequal to zero were selected and its reconstruction via BPDN. In this example, the relative RMS reconstruction error resulted in 0.14.

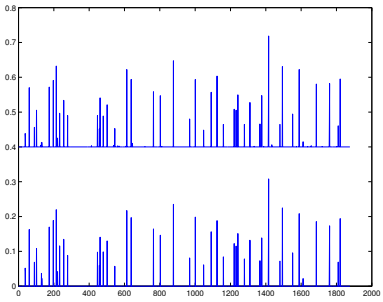

Fig. 8. *A simulated sparse scene ($S = 50$) arranged as a 1D sequence corresponding to the chosen 1876 directions and the reconstruction with basis pursuit denoising*

We used also images for the simulation of reflectivities. The phases were drawn uniformly over $[0, 2\pi)$. An exemplary result is shown in Fig. 9.

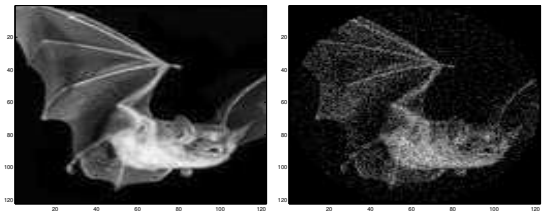

Fig. 9. *Left: a gray level photo as source for the assumed reflectivity. Right: An image obtained by compressive sensing based on the simulated roulette-radar measurements*

VII. Summary and Outlook

The experimental system is shortly before the first measurements. There will be different options with respect to the radar units with respect to frequency (80,120,220 and 300 GHz) and bandwidth (0 to 40 GHz). Parallel to finishing the measurement equipment electromagnetic analysis is performed to refine the elementary signal models introduced in section (V).

Acknowledgements

The authors would like to thank Sven Augustin and his colleagues for fruitful discussions, Thanh Nhat Luong and the workship of ZESS for the design and manufactoring of the mechanical devices and FHR for the preparation of the measurements.

References

[1] M. F. Duarte, M. A. Davenport, D. Takhar, J. N. Laska, T. Sun, K. F. Kelly, and R. G. Baraniuk, "Single-pixel imaging via compressive sampling," *IEEE Signal Processing Magazine*, vol. 25, no. 2, pp. 83–91, March 2008.

[2] J. Haupt and R. Nowak, "Signal reconstruction from noisy random projections," *IEEE Transactions on Information Theory*, vol. 52, no. 9, pp. 4036–4048, Sept 2006.

[3] S. Augustin, S. Frohmann, P. Jung, and H. W. Hübers, "An optically controllable 0.35 thz single-pixel camera for millimeter resolution imaging," in *2017 42nd International Conference on Infrared, Millimeter, and Terahertz Waves (IRMMW-THz)*, Aug 2017, pp. 1–2.

[4] S. Augustin and H. W. Hübers, "Understanding mask switching for thz compressive imaging," in *2016 41st International Conference on Infrared, Millimeter, and Terahertz waves (IRMMW-THz)*, Sept 2016, pp. 1–2.

[5] Z. Zhang, L. Liu, A. A. B. Sajak, L. Gan, Y. Huang, and Y. Shen, "Spinning disk as a spatial light modulator for rapid infrared imaging," *IET Microwaves, Antennas Propagation*, vol. 11, no. 3, pp. 317–323, 2017.